Integration of a piezoresistive microprobe into a commercial gear measuring instrument

Short title: **Integration of a microprobe into a CMM**

D. Metz[1], N. Ferreira[1], J. Chaillot[2], M. Stein[2], K. Kniel[2], A. Dietzel[1]

[1] TU Braunschweig, Institut für Mikrotechnik (IMT); Alte Salzdahlumer Str. 203, 38124 Braunschweig, Germany

[2] Physikalisch-Technische Bundesanstalt (PTB); Bundesallee 100, 38116 Braunschweig, Germany

Corresponding author: D. Metz, d.metz@tu-braunschweig.de;

phone: +49 531 391-9743; fax: +49 531 391-9751

Abstract – Various microprobes have been developed in the last decade to address the needs of micrometrology. However, most microprobes are only employed in specialized measuring machines located in a few research institutes and are not widespread in the industry. This work aims to extend the capabilities of conventional coordinate measuring machines (CMMs) towards measuring microgeometries through the low-cost integration of a tactile microprobe. In order to demonstrate this, a gear measuring instrument (GMI), which is a commercial CMM not specialized for measurements at the microscale, has been equipped with a recently developed silicon-membrane-based microprobe. In the first part of this work, the working principle of the microprobe, its assembly and its integration into the GMI are described. Two different mounting setups of the microprobe onto the GMI were evaluated and tested. Measurements on the GMI were performed solely with the microprobe or by combining the microprobe and the measurement system already present on the GMI. This combination makes it possible to use the microprobe advantageously and to exchange it in a comfortable semi-automatic way. To test these two mounting setups, a new involute scanning artifact (SAFT) with superimposed waviness was measured.

1   Introduction

The need to measure microgeometries is increasing due to progressing miniaturization and the increasing degree of the integration of functions into technical systems. In the last decade, various tactile microprobes have been developed on the basis of different physical sensing principles [1,2]. These microprobes are used to determine the geometry of a workpiece with very small characteristics, by sensing the deflection of a probing element (e.g. a probing ball on a stylus) in contact with the workpiece. For nondestructive or pseudo noncontact probing, vibrating microprobes have been developed [3,4]. More recently, a capacitive vibrating microprobe was developed at TU Ilmenau [5] and the piezoelectric vibrating microprobe by Mitutoyo [1,6] and by the UK's National Physical Laboratory (NPL) [7]. The glass fiber microprobe made by Werth (Werth GmbH, Germany), based on a development of the Physikalisch-Technische Bundesanstalt (PTB), combines tactile probing with the optical evaluation of the probing ball deflections. An ultra-small probing stylus made from a glass fiber with a probing ball diameter down to 20 µm is used for 2D and 3D measurements with ultra-small probing forces down to 20 µN [8–10]. A similar approach has been taken at the US National Institute of Standards and Technology (NIST) leading to the so-called Fiber Deflection Probe, for measuring Ø100 µm wide and 5 mm deep holes with a claimed repeatability of 0.07 µm [11]. At the Swiss Federal Institute of Metrology (METAS), a microprobe, based on a three-parallelogram kinematic structure combined with inductive sensors and active actuators, provides an isotropic mechanical behavior with a stiffness down to 20 N·m^{-1} and large measuring ranges of up to ±200 µm. A three-legged microprobe has been developed at NPL made out of three beryllium–

2

copper flexures, assuring the movability of a stylus placed in its center and the isotropic mechanical behavior of the system with small stiffness (10 N·m^{-1}). This sensor, available at IBS (IBS Precision Engineering, The Netherlands) provides a resolution of 3 nm using three capacitance sensors [12–15]. Another three-legged microprobe has been developed at Eindhoven University of Technology (commercially available through XPRESS Precision Engineering B.V., The Netherlands) based on a silicon suspension combined with piezoresistive sensors. It provides a repeatability of 4 nm and probing forces down to 0.01 mN [16–18]. The silicon-membrane-based microprobe used in this work has been developed at the Technische Universität Braunschweig (TU Braunschweig) in cooperation with PTB [19–24]. Depending on the probing direction, this microprobe provides a resolution of 3-5 nm and a repeatability of 10-20 nm with a stiffness of 1-20 mN·µm^{-1} [19,23]. Zeiss built the F25 [25], a micro-coordinate measuring machine (µCMM), using the almost same type of microprobe. This specialized machine can enable a measurement uncertainty in sub-micrometers, but is no longer commercially available. The utilization of such microprobes, even when commercially available, is often limited to measurements on prototype measuring machines or on specialized and expensive µCMMs. Measurements of microgeometries, which require a tip diameter smaller than 300 µm or even 1 mm, are usually not possible on conventional CMMs. This limitation is imposed because of the difficulty of using such a small stylus and not because of the machine accuracy. In order to extend the measurement capabilities of conventional CMMs towards micro-measurements, efforts for the integration of silicon-membrane-based microprobes into a CMM started five years ago at IMT and at PTB [24,26,27]. In order to improve the performance of this microprobe integrated into the CMM, an optimization of the assembly and integration process was developed and validated in this work. The microprobe employed is described in Section 2, and was implemented on a GMI, the P40 made by

3

Klingelnberg GmbH. This machine is equipped with three linear axes and a rotatory table and is designed to measure gears and other axially symmetric workpieces [28]. The combination of a microprobe and a GMI has made possible for measuring geometries with a small tip diameter down to 50 µm [23,29]. In the first part of this work, the microprobe, its working principle, its production and its new assembly, and its properties are presented. In the second part, the integration into the GMI is explained, as well as the preparation procedure needed before measurements. A new mounting setup of the microprobe onto the GMI is introduced and compared to the previous one, which has some limitations. The last part of this paper concerns the validation of this integration concept using a novel involute waviness scanning artifact.

2 Silicon-membrane-based microprobe

2.1 Working principle

The microprobe is composed of a 25 µm thin silicon cross membrane, on which a stylus is mounted. For its integration, the silicon chip was fixed and contacted on a printed circuit board (PCB), which provided a stable support for the fixation and allowed contact with the back of the microprobe (Figure 1a). During the tactile probing, transversally oriented piezoresistors were utilized to determine the stylus deflections (Figure 1b and c). In groups of four, the piezoresistors are connected to each other to form a Wheatstone bridge on each membrane side, marked A, B, C and D (Figure 1b). These four bridges, electrically contacted via copper pads, deliver four measurement voltages U_A, U_B, U_C, U_D, which are linearly dependent on the deflections of the stylus m_x, m_y, m_z in the coordinate system of the microprobe R_m (x, y, z). In Figure 1c, the mechanical deflections in the microprobe are illustrated for the main directions. The mechanical stresses assume maximum positive or negative values at indicated positions where piezoresistors are placed. Through a force in the z-direction, all four membrane

4

bridges A, B, C and D are deformed in the same way and deliver a signal change. Forces in the x- and y-directions lead to a tilting of the membrane. The membrane bridges oriented parallel to the deflecting force deliver a signal change with an opposite sign. The other two bridges are under torsion, which induces no signal changes [22].
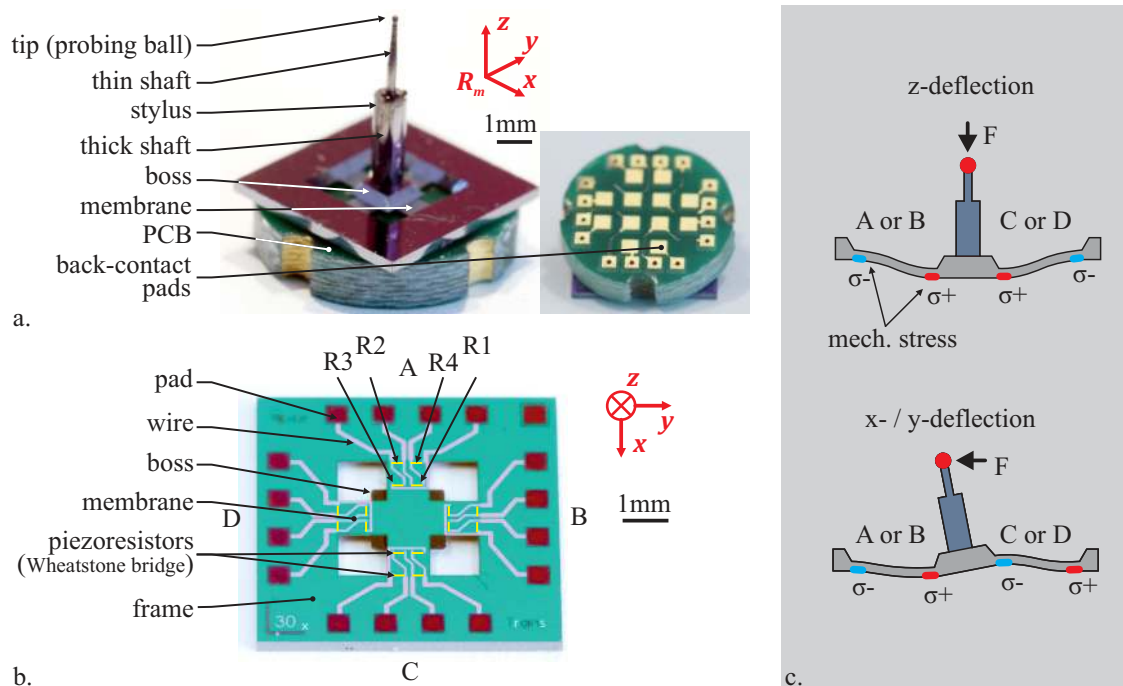

Figure 1 – a. Mounted microprobe on a PCB with a stylus tip with a diameter of 250 µm and back view of the PCB with the contacting pad grid, b. bottom of an silicon chip with a cross membrane and the piezoresistors, and c. sketch of the working principle of the silicon-membrane-based microprobe.

As a consequence of this working principle [20,22,23,26,30], the four measured voltages can be transformed into three theoretical main axis signals U_x', U_y', U_z' with the help of the matrix T (Eq. 1).

$$\begin{pmatrix} U_x' \\ U_y' \\ U_z' \end{pmatrix} = T \cdot \begin{pmatrix} U_A \\ U_B \\ U_C \\ U_D \end{pmatrix}, \qquad with\ T = \begin{bmatrix} 1 & 0 & -1 & 0 \\ 0 & 1 & 0 & -1 \\ 1 & 1 & 1 & 1 \end{bmatrix} \qquad 1$$

These three main axis signals are directly proportional to the three deflections m_x, m_y, m_z, where c_x, c_y, c_z in mm·V^{-1} are the respective constants of proportionality (Eq. 2). The conversion matrix C composed of c_x, c_y, c_z was obtained during an initial characterization of the microprobe.

5

$$\begin{pmatrix} m_x \\ m_y \\ m_z \end{pmatrix}_{R_m} = C \cdot \begin{pmatrix} U_x' \\ U_y' \\ U_z' \end{pmatrix}, \qquad with\ C = \begin{bmatrix} c_x & 0 & 0 \\ 0 & c_y & 0 \\ 0 & 0 & c_z \end{bmatrix} in\ mm \cdot V^{-1} \qquad 2$$

The transformation matrix T contains non-diagonal elements, which is a consequence of the working principle. In previous characterization experiments [27], very little cross talk was observed and least squares fits revealed non-diagonal elements in C with values in the range of only 0.1 - 4.5 % of the diagonal elements. In practice, however, measurements on the GMI do not differ whether diagonal elements are considered or not and all non-diagonal elements of C can be set to zero [22–24,26].

2.2 Fabrication and assembly

The silicon chip is made from a double-side polished silicon wafer with a (100) crystal orientation and a thickness of 360 ± 25 µm. In a first step, the piezoresistors are diffused in the silicon by a double boron doping process. After passivation with a silicon dioxide (SiO_2) layer, they are wired by aluminum tracks through vias structured in the SiO_2 layer. To protect the wiring, a silicon nitride (Si_3N_4) layer is employed. Then 20 µm thick soldering Cu pads are deposited by galvanization on the tracks for further external contacting (Figure 2, Step 1). In a second step, a double layer of SiO_2 and Si_3N_4 is employed as a hard mask during the wet etching of the silicon in a 40 % potassium hydroxide (KOH) solution at a temperature of 80 °C to realize the thin membrane. The membrane thickness is controlled by knowing the etching rate over the processing time. The cross form of the membrane is obtained by a DRIE etch process [23,26] (Figure 2, Step 2). After the wafer-level processing of the silicon membrane, the chips are separated by wafer dicing. Each silicon membrane is then flip-chip mounted by being soldered onto a PCB which leads to a robust and compact probe system. With the help of a positioning tool and a surface mounted device (SMD) stencil, a low-temperature solder paste (melting temperature 135 °C) is deposed on the soldering pads of the

6

membrane. Then, the chip is positioned on the PCB and heated up on a hotplate (set temperature 150 °C). Capped 105 µm high vias in the PCB were employed as contact pads in order to reduce the diameter of the PCB to 8 mm (Figure 2, Step 3). Finally, the stylus is mounted onto the middle of the membrane with epoxy glue (353ND, Epothek) [30]. Styli with ruby spheres of diameters between 300 µm and 120 µm are commercially available. Styli with tips down to 50 µm diameter can be produced using wire electro-discharge grinding (using SX200 from Sarix) as detailed in [23,29]. Through this process, a tungsten carbide rod is eroded in the desired form by means of electro-discharge with a constant feed wire.
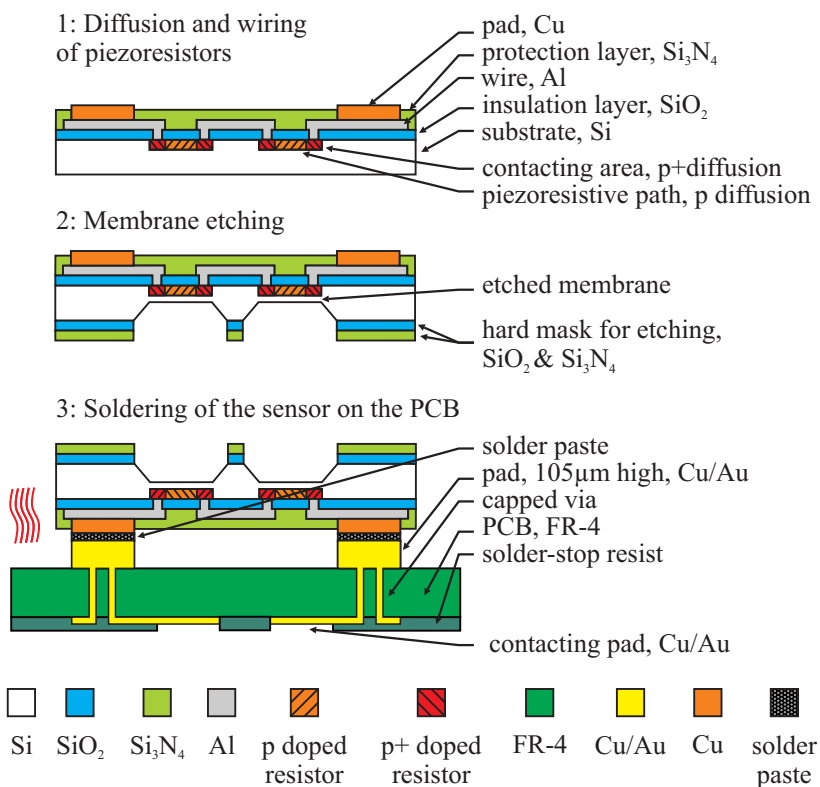

1: Diffusion and wiring of piezoresistors
- pad, Cu
- protection layer, Si₃N₄
- wire, Al
- insulation layer, SiO₂
- substrate, Si
- contacting area, p+diffusion
- piezoresistive path, p diffusion

2: Membrane etching
- etched membrane
- hard mask for etching, SiO₂ & Si₃N₄

3: Soldering of the sensor on the PCB
- solder paste
- pad, 105µm high, Cu/Au
- capped via
- PCB, FR-4
- solder-stop resist
- contacting pad, Cu/Au

Si   SiO₂   Si₃N₄   Al   p doped resistor   p+ doped resistor   FR-4   Cu/Au   Cu   solder paste

Figure 2 – Production of silicon membrane with integrated piezoresistive sensors and compact flip-chip mounting on a PCB.

2.3   Microprobe properties

The microprobe design is the result of numerous works, which also provide details of its properties [20–24,26,30]. The microprobe exhibits a mechanical anisotropy with its stiffness in the z-direction being larger than in the xy-plane. For deflections in the z-direction and in the xy-plane, the deformation states induced in the membrane, the

7

number of reacting signals (4 vs 2), and as a consequence also the sensitivities differ. An extensive analysis has been performed, in which the geometries of the membrane and the stylus have been varied to study respective influences on the stiffness and on the sensitivity of the microprobe [23,26]. In Table 1, data from two microprobes (1 and 2) with different probing ball and styli together with data from microprobe (3) of this study are listed. The styli are composed of a shaft with two segments; a thick one with a 1 mm diameter, and a thin one with a 300 µm diameter as well as a tapered element holding the probing ball (Figure 1a). All three microprobes exhibit a high mechanical anisotropy leading to slipping of the tip when the probe deflects in an axial (z) direction and at the same time in a non-axial direction of the stylus (x, y). Through this slipping, the measurement uncertainty increases. Smaller stylus tips lead to lower sensitivities. Mechanical anisotropy can be completely avoided using stacked suspensions [26] or using a completely different probe design based on stacked parallelogram displacement sensors [31]. The measuring range is limited by the deflection leading to fracturing, which was investigated in earlier studies on microprobes 1 and 2 [23,26]. The measurements of the scanning artifact (SAFT) as described below did not need an extra small tip diameter. A stylus with a probing ball diameter of 250 µm and a long total length of 7.5 mm was chosen in order to obtain a sufficient sensitivity for submicron resolution with maximum accessibility.

The measurement uncertainty of a microprobe is affected by various influences, among them the number and the quality of the signals employed (noise), the microprobe sensitivities and stiffness, and the characterization of the microprobe. As the sensitivity in z is more than twice as high as in the xy-direction, the influence of signal noise is lower in z. Furthermore, the deflections in z are determined out of four signals instead of two in the xy-direction. A noise level of up to 0.6 mV was determined earlier [26] for

the present setup, which induces displacement uncertainties of up to 91 nm in the xy- and 24 nm in the z-direction for the microprobe used.

Table 1 – Properties of silicon-membrane-based microprobes of earlier works [23,26] (microprobes 1 and 2) and this work (microprobe 3).

Microprobe	1	2	3
Membrane thickness in µm	43	43	25
Probing ball diameter in µm	300	50	250
Transition diameter in mm	250	40	180
Total stylus length in mm	5	5	7.5
Stiffness in xy in mN·µm^{-1}	1.71	0.97	0.247
Stiffness in z in mN·µm^{-1}	32.9	16.99	13.9
Fracture deflection in z /xy in µm	50 / 110	10 / 40	Not available
Sensitivity in xy in mV·V^{-1}·µm^{-1}	4.33	1.20	2.63
Sensitivity in z in mV·V^{-1}·µm^{-1}	26.5	18.6	20.0

3   Integration of the microprobe into a GMI

3.1   Description of the GMI

The GMI P40 made by Klingelnberg GmbH consists of thee linear axes (X, Y, Z), which define its coordinate system R_{40}, and of a rotation axis C (in the Z-direction) realized by a rotary table, on which the workpieces are placed (Figure 3a). The probing head (M44) of the GMI placed in the quill has a coupling system, which enables the automatic exchanging of the stylus. In Figure 3b, the standard measurement setup of the P40 with a –Z stylus is presented. Each stylus is fixed on a changing plate, which fits to the coupling system present on the free end of the probing head. During the tactile measurements, the tip of the stylus comes into contact with the workpiece, which induces deflections in the three directions of the probing head. These deflections M_X, M_Y, M_Z and the positions of the probing head P_X, P_Y, P_Z allow the geometries of the workpiece to be determined. The measuring accuracy of the P40 for gear measurement can be found in [32] and [33], accuracy class I.
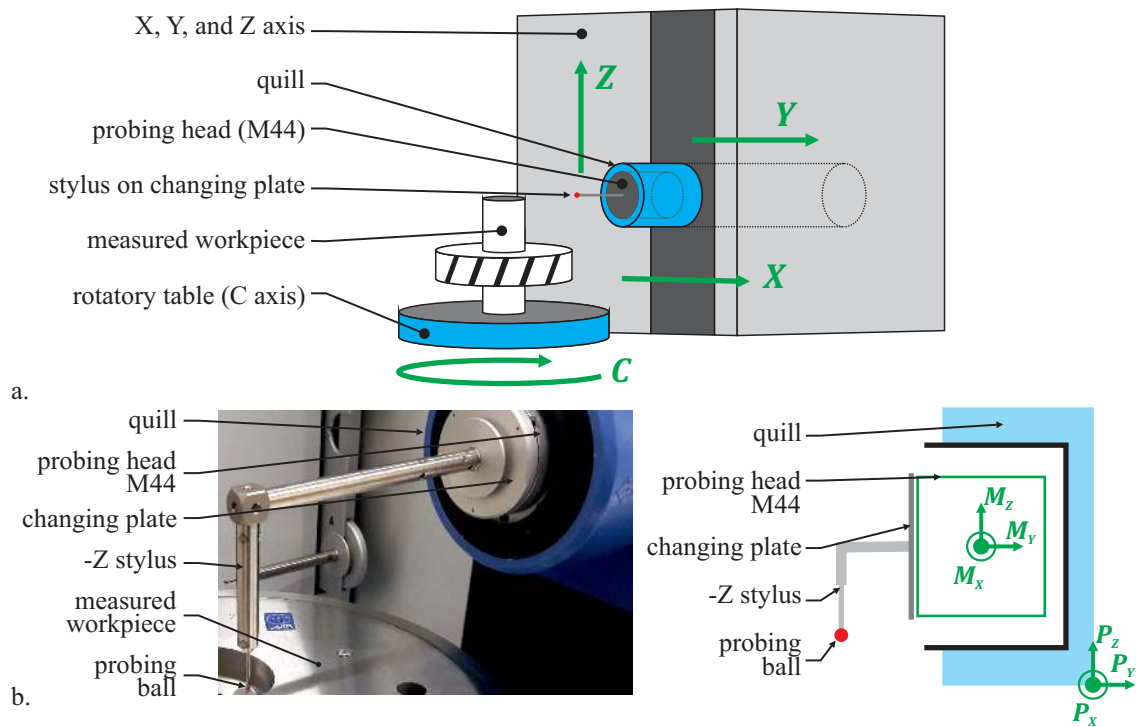
9

Figure 3 – a. Diagram of kinematics and main components of the GMI, P40, and b. detail and schematic diagram of the standard setup of the GMI with the probing head M44 and a standard –Z-stylus.

3.2 Electrical and mechanical interface of the microprobe

The microprobe was mounted onto a changing plate with a special adapter, which enables it to be mechanically fixed onto the GMI (onto the M44) and also allows it to have electrical contact. The adapter is composed of a cartridge and a holder (Figure 4). The microprobe on a PCB is clamped via screws in the cartridge, which is plugged into and screwed onto the holder. Contact springs ensure the contacting of the back-contact pads of the PCB. The new mounting screwing system (mounting screw and anti-rotation nut in Figure 4) of the cartridge offers the advantages of an easy, comfortable and robust microprobe exchange, without the risk of damage. Also, the orientation of the microprobe can be changed (0° to 90°) thanks to the rotation axe and the position screws. In this work, only the 90° orientation was investigated. In comparison with the previous version of this adapter [26,27], the external diameter was reduced from 16 mm to 10 mm to allow access to smaller structures, and its utilization was made more comfortable (screwing system).

10
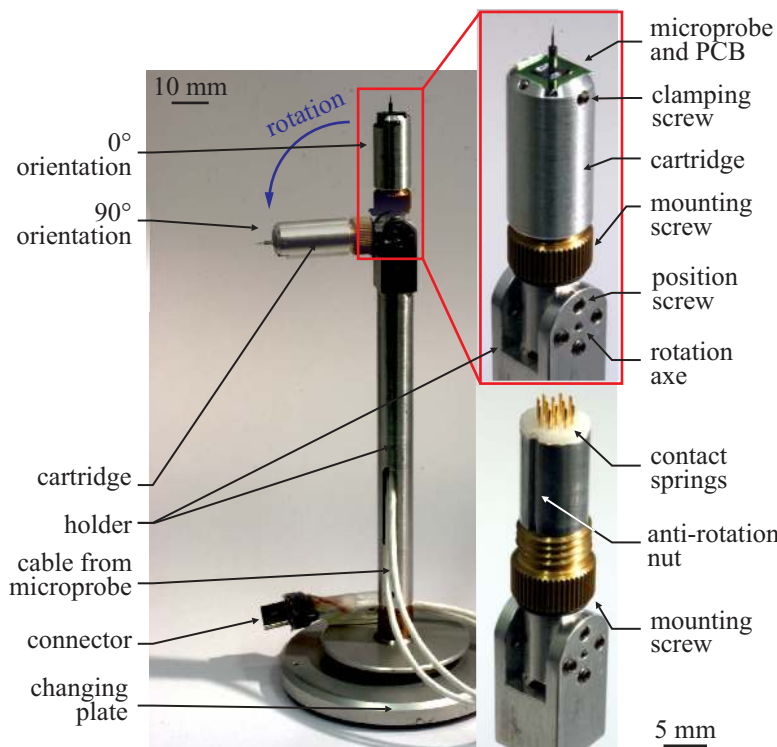
Figure 4 – Novel adapter for the microprobe with a detailed view of the electrical and mechanical interfacing of the microprobe.

3.3 Installation setups of the microprobe

The microprobe, mounted in its adapter, was installed in series onto the probing head (M44) via a changing plate just like one of the conventional styli. Two installation setups were investigated. In the first one, denoted by MC, the microprobe was attached to the probing head, so that both measuring systems were employed (Figure 5a). In the second one, denoted by MA, the probing head was clamped with the help of a ring to mechanically deactivate the P40 measuring system (Figure 5b). Depending on the orientation of the microprobe, the measured deflections had to be rotated to match the GMI coordinate system R_{40} (Eq. 3 and Figure 5). For the 90° orientation (Figure 4), the rotation matrix R from $R_m\ (x,y,z)$ to $R_{40}(X,Y,Z)$ is equal to the identity matrix I_3.

$$\begin{pmatrix} m_X \\ m_Y \\ m_Z \end{pmatrix}_{R_{40}} = R \cdot \begin{pmatrix} m_x \\ m_y \\ m_z \end{pmatrix}_{R_m} \qquad\qquad 3$$

In MC setup, the microprobe and the M44 were used simultaneously, and for the undisturbed movability of the probing head, a flexible cable made of a thin polyimide

11

film helped with transmitting the voltages of the microprobe U_A, U_B, U_C, U_D (Figure 5a).

For this setup case, the sum of the deflections of the microprobe m_X, m_Y, m_Z and of the

probing head M_X, M_Y, M_Z was considered during the measurements. In the following,

this deflection sum is called MC_X, MC_Y, MC_Z. For the MA setup, only the deflections

m_X, m_Y, m_Z were considered during measurements as the movements of the M44 were

disabled by using a clamp ring (Figure 5b), so that the microprobe could be employed

solely in the GMI as in previous works. This last case is especially necessary for the

characterization of the microprobe in the GMI but does not allow a fast exchange

between the microprobe and a standard stylus. These two setups were compared to

evaluate their influence on the measurement results, their advantages, and

disadvantages.
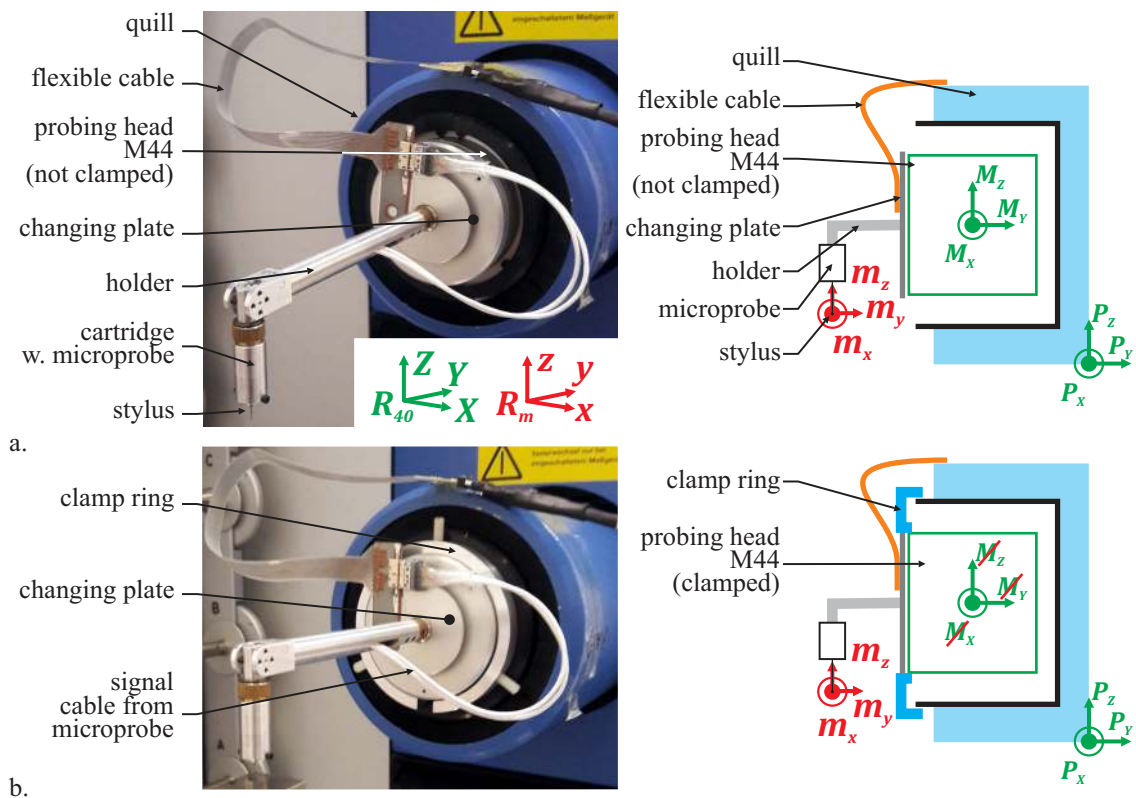
Figure 5 – Installation of the microprobe on the P40; a. on the free probing head of the P40 (MC setup) and b. on the clamped probing head (MA setup).

3.4   Evaluation of the microprobe signals

The four voltages U_A, U_B, U_C, U_D of the microprobe were transmitted by cables to the GMI. Thanks to data acquisition modules (DAQP-BRIDGE-A from Dewetron), the signals were pre-amplified (with a gain of 10) and pre-filtered (low pass frequency 100 Hz), and the supply voltage for the Wheatstone bridges was delivered (supply voltage 5V). In the GMI, the voltages were digitalized and converted into deflections m_X, m_Y, m_Z using the matrices T, C and R (Eq. 1, Eq. 2 and Eq. 3). On an external PC, the signals were monitored on a LabVIEW® program, which also permits setting the DAQ modules and running the offset compensation of the signals on the modules. In Figure 6, the signal processing path is presented, with the different components, their functions, and associated signals.
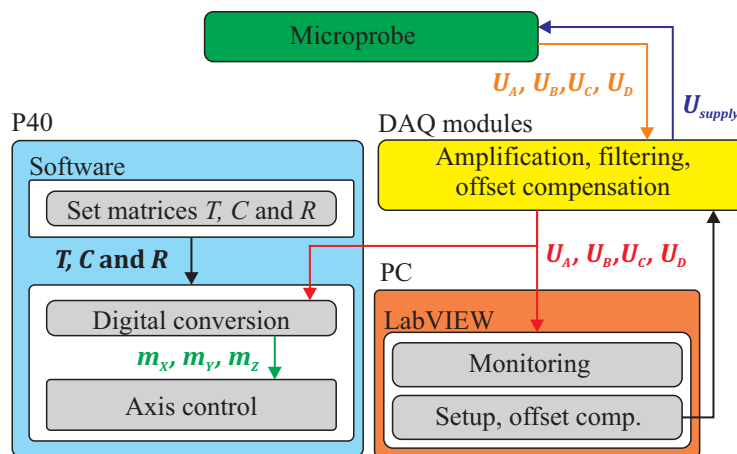
Figure 6 – Processing of the signals of the microprobe to the GMI.

4   Characterization of the microprobe

Before using the microprobe in the GMI, the conversion matrix C (coefficients c_x, c_y, c_z) has to be determined to obtain the relation between the deflections of the stylus m_x, m_y, m_z and the measured voltages U_A, U_B, U_C, U_D.

13

4.1 Determination of the conversion matrix

The microprobe was characterized by inducing deflections in its orthogonal directions (x, y, z) in contact with a small reference cube (Figure 7) [20,27]. The characterization was made with a cubic artifact instead of a sphere, to avoid the slipping of the tip when the probe deflects in the axial and at the same time in a non-axial direction of the stylus. The cube was aligned with the main directions of the probe, which are the main axes of the machine, using the scanning alignment tool of the machine within a tolerance of less than 1°. For the characterization, the clamp ring was employed (MA setup) to ensure that only the microprobe deflects.

a.   b.
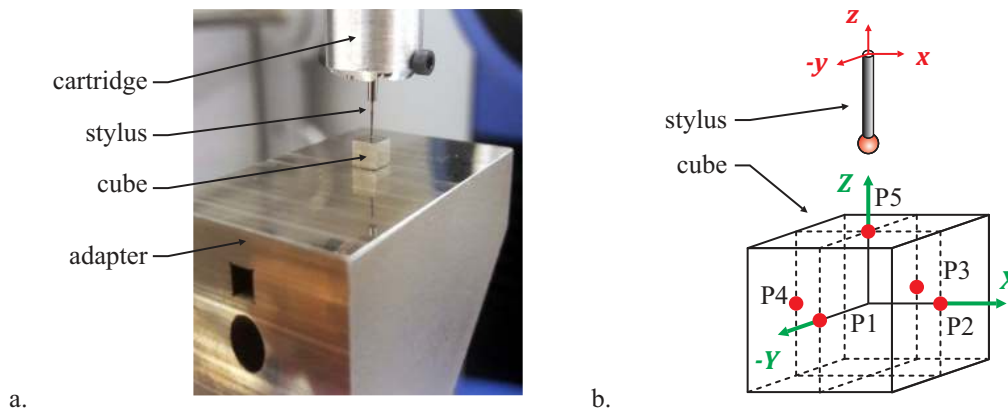
Figure 7 – a. Microprobe deflecting in the z-direction on a small reference cube, and b. sketch of the small reference cube with the probed points P1-P5.

During the automatic characterization, five points were probed on the cube (Figure 7b), one for each main axis deflection of the microprobe; $\pm x$ (P2, P4) , $\pm y$ (P1, P3) and z (P5, probed twice). At each point, the tip was brought into contact with the cube and deflected step by step. Simultaneously, the M44 positions P_X, P_Y, P_Z and the signals $U_x{}', U_y{}', U_z{}'$ were recorded. The real deflections of the microprobe m_X, m_y, m_Z were assimilated into the displacements of the microprobe in the CMM D_X, D_y, D_Z, which were calculated out of P_X, P_y, P_Z. Through a linear regression of $D_i = c_i \cdot U_i{}'$, the conversion coefficients (slopes) between the real deflections and the signals were determined, as illustrated in Figure 8 for the x-direction.
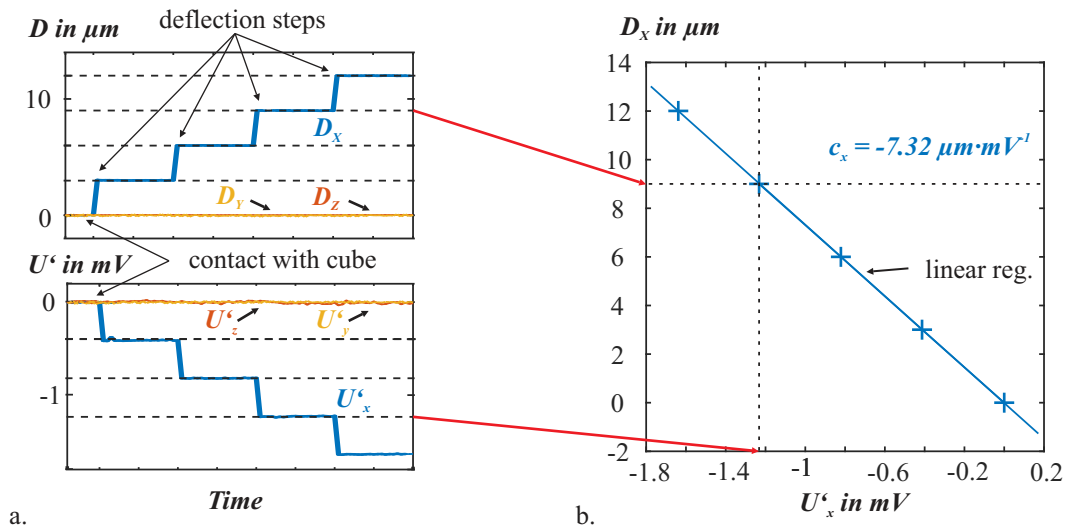
14

Figure 8 – Determination of c_x by linear regression using $D_x = c_x \cdot U_x'$; a. evaluation of values of D_x and U_x' for each deflection step and b. plot of the linear characteristic between D_x and U_x'.

Each coefficient (c_x, c_y, c_z) was determined out of the results of the two corresponding points (i.e. P2 and P4 for c_x). In Eq. 4, the conversion matrix C with the obtained mean values is given.

$$C = \begin{bmatrix} 7.26 & 0 & 0 \\ 0 & 7.98 & 0 \\ 0 & 0 & 0.999 \end{bmatrix} \cdot 10^{-3} \; in \; mm \cdot V^{-1} \qquad 4$$

In order to evaluate and compare the two mounting setups (MA and MC), the characterization was repeated during the stepwise deflection of the microprobe by recording the M44 positions P_X, P_Y, P_Z, together with the deflections m_X, m_Y, m_Z calculated from the microprobe signals for the MA setup (Eq. 2 and Eq. 3) and the calculated deflection sum MC_X, MC_Y, MC_Z for the MC setup (3.3.3.). To compare the deflections of the microprobe tip D_X, D_Y, D_Z, calculated from P_X, P_Y, P_Z, with the recorded ones (m, MC), a linear regression was carried out. In Eq. 5 and Eq. 6, the results of the regression are presented for both setups. In the case of a perfect conversion / characterization, the matrix should be equal to the identity matrix I_3.

For the MA setup

$$\begin{pmatrix} D_X \\ D_Y \\ D_Z \end{pmatrix}_{R_{40}} = \begin{bmatrix} 1.001 & 0 & 0 \\ 0 & 0.831 & 0 \\ 0 & 0 & 0.963 \end{bmatrix} \cdot \begin{pmatrix} m_X \\ m_Y \\ m_Z \end{pmatrix}_{R_{40}} \qquad 5$$

For the MC setup

$$\begin{pmatrix} D_X \\ D_Y \\ D_Z \end{pmatrix}_{R_{40}} = \begin{bmatrix} 1.015 & 0 & 0 \\ 0 & 0.875 & 0 \\ 0 & 0 & 0.975 \end{bmatrix} \cdot \begin{pmatrix} MC_X \\ MC_Y \\ MC_Z \end{pmatrix}_{R_{40}} \qquad 6$$

The two setups can be considered as equivalent as their conversions are equal within an error lower than 5 % in all axes (lower than 1.4 % for the X-direction). In the X-direction, the calculated deflections of the MA setup are 0.1 % smaller than the real deflections D and 1.5 % smaller for the MC setup. In the Y- and Z-directions, the calculated deflections are even smaller (up to 17 % difference with the real deflections D). A lower error in the X-direction than in the Y- and Z-directions can be explained by the stage oscillating around a target position in the Y- and Z-directions, which is non-detectable in the X-direction. The moving mass for the X-stage is larger than on the other ones (see the kinematics of the GMI, Figure 3a) and acts as a low pass filter. For the following involute profile measurements, the poor conversions in the Y- and Z-directions are not relevant. During the measurement of a gear, only a deflection in the X-direction occurs. The conversions could be improved through an iteration of this characterization. To this end and for correct 3D measurements, further investigations have to be undertaken. During the measurement, it was observed that the MC setup offers some advantages over the MA setup. The microprobe has strong mechanical anisotropy, which causes a source of measurement uncertainty through the probing of inclined surfaces [34]. The stiffness in the z-direction (ca. 20 N·mm^{-1}) is about 20 times larger than in the other two directions (ca. 1 N·mm^{-1}) [26]. Also, it permits a limited range of deflection of about 50 µm in the z-direction and ±110 µm in the other directions. The probing head (M44) has an isotropic mechanical behavior with

16

a stiffness of 0.75 N·mm^{-1} and a deflection range of ±1 mm. Through the combination of the microprobe and the M44, the anisotropy and the limited deflections of the former can be, in part, compensated for by the latter. For example, through a deflection in the *z*-direction, it was observed that the probing head M44 deflects the most. Moreover, without the clamp ring, an easy and semi-automatic exchange between the microprobe and a standard stylus can be realized, as required for industrial use.

4.2 Referencing on the machine

Before measurements can be performed, a referencing procedure is required. During this standard procedure on the GMI, the position of the stylus tip in the machine coordinates system and its diameter are determined and stored as reference data. Therefore, a 2 mm reference sphere with a calibrated diameter was probed. Five different points on the sphere were probed twice at two different positions of the sphere on the rotatory table (0° and 180°) in order to compensate for the rotational errors of the table [24]. The probing points are pre-determined depending on the stylus direction. In Figure 9, the setup of the referencing with the reference sphere in the case of combined probing systems (MC setup without clamp ring) and the probed points on the reference sphere for a –Z stylus are shown.

In the case of the MC setup, the reference data can be simply re-loaded after installing the microprobe onto the machine. For the MA setup, referencing has to be re-run after each installation, because of the manual adjusting of the clamp ring.
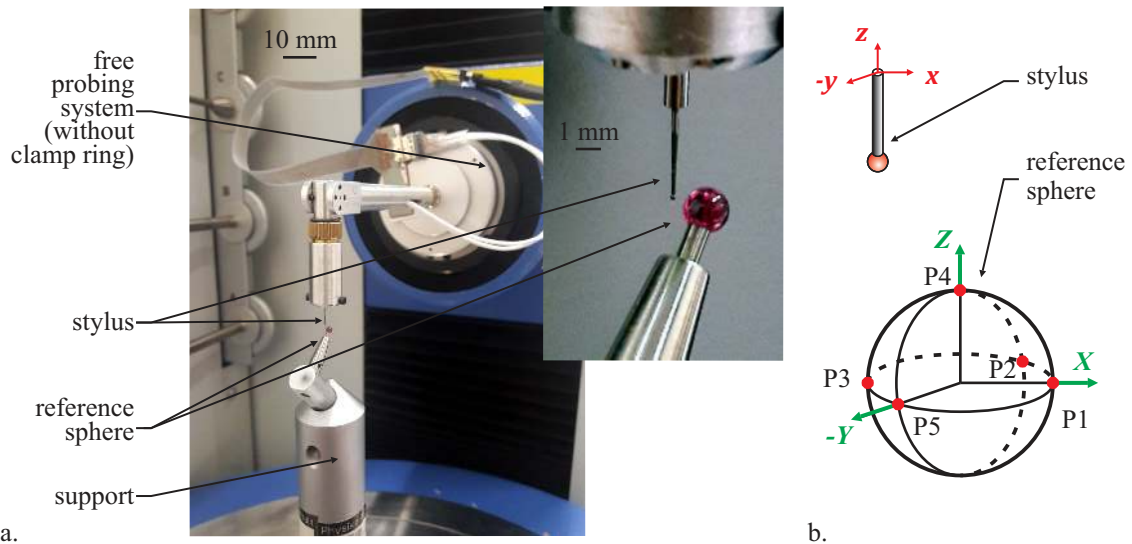
Figure 9 – Referencing setup of the microprobe with the MC setup and a detail of the reference sphere, and b sketch of the reference sphere with the five probed points.

5   Involute scanning artifact

In order to test and validate the microprobe integration procedure and the new setup, a special gear artifact was measured. In this section, details of its design are presented.

5.1   Description of the artifact

Recently, two novel SAFT artifacts were developed and produced at PTB to investigate the influence of scanning parameters during gear profile measurement. A sketch of one SAFT is shown in Figure 10. Each artifact is composed of an internal (5) and an external (6) involute shape, embodying the typical gear profile. The profiles of the first one are superimposed with a certain waviness (SAFT2w), while the second has a smooth surface (SAFT3g). The standards have been manufactured from a 20 mm thick piece of C45 steel with a diameter of 290 mm. They are endowed with a reference circle (2) and a reference plane (3) defining the *z*-axis of the workpiece coordinate system. A reference hole (4) indicates the position of the *x*-axis. A 90° segment of the involute's base circle (7) with a radius r_b = 20 mm is also embodied. A point on the datum face (1) serves as a reference for the height defining $z = 0$.
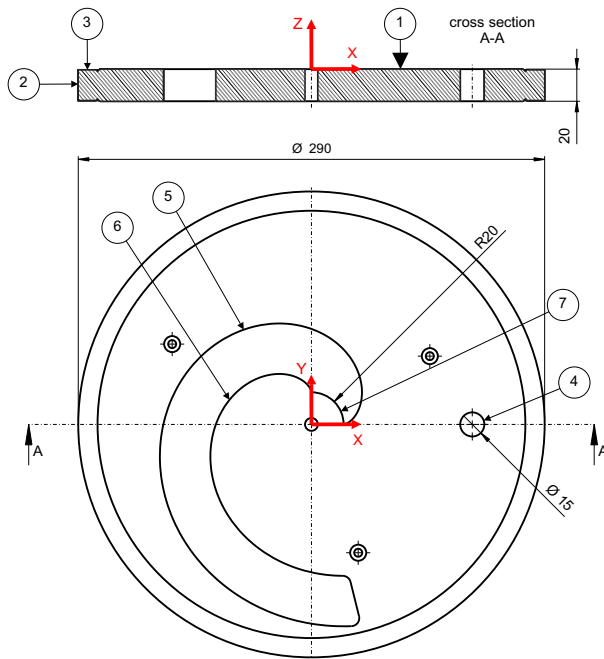
Figure 10 – Technical drawing of the involute waviness scanning measurement standard.

The involute profiles have been cut with a wire electro-discharge machining process.

An optimal surface quality of the profiles with $R_a \leq 100$ nm required up to eight cutting

steps from the rough to the superfinishing stages. The references have been machined

by a conventional turning and grinding process, in order to obtain suitable polished

surfaces. The artifacts are mounted onto a special base frame composed of a bottom disc

and three supporting cylinders (Figure 11). This enables easier handling, positioning

and centering of the parts on the rotary table of the P40.
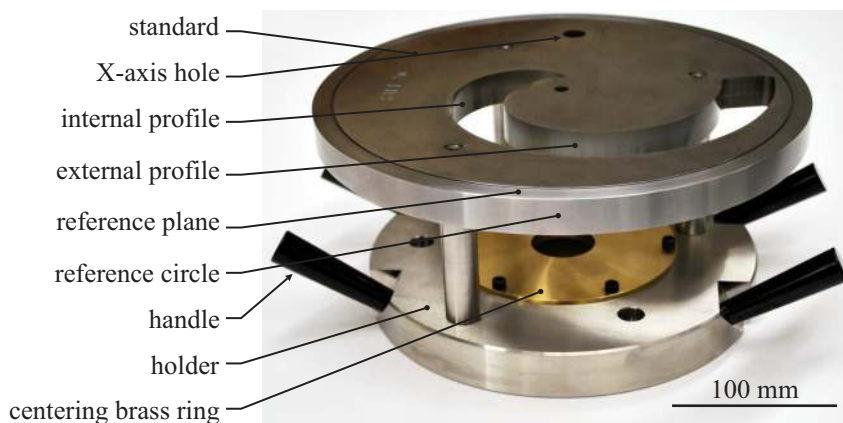
Figure 11 – Involute scanning artifact (SAFT) mounted on its holder.

5.2 Mathematical definition of an involute curve with waviness

To determine the desired profile for each involute without or with waviness, the following mathematic equations have been employed [35]. Figure 12 shows the parameters for the definition of the involute curve and superimposed waviness.
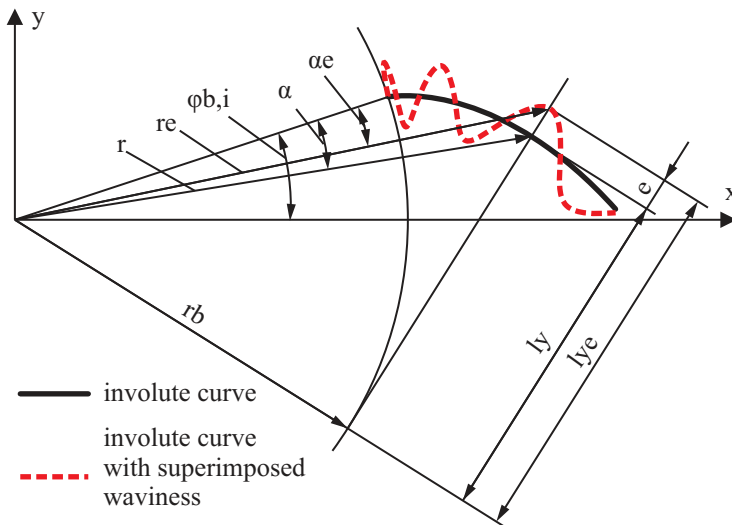
Figure 12 – Scheme of an involute curve with superimposed waviness and its parameters [35].

The involute gear profile is defined by the following equation depending on the length of roll [36]:

$$\begin{pmatrix} x \\ y \end{pmatrix} = \begin{pmatrix} r \cdot \cos(\varphi_b + inv\ \alpha) \\ r \cdot \sin(\varphi_b + inv\ \alpha) \end{pmatrix} \qquad\qquad 7$$

with:

- r :   radius

$$r = \sqrt{r_b^2 + l_y^2} \qquad\qquad 8$$

- r_b: base circle radius

- l_y :   length of roll

- φ_b :   position angle of the involute origin at base circle

- $inv\ \alpha$:   involute angle

$$inv\ \alpha = tan\left(arccos\left(\frac{r_b}{r}\right)\right) - arccos\left(\frac{r_b}{r}\right) \qquad\qquad 9$$

Analogously, the following equivalent equation of an involute curve with waviness can be deduced from Eq. 7 and Figure 12 [35,36]. It is important to consider that the gear

20

profile waviness is related to the length of roll l_y as this reflects the functional behavior of the gear.

$$\begin{pmatrix} x \\ y \end{pmatrix} = \begin{pmatrix} r_e \cdot cos(\varphi_b + inv\,\alpha_e) \\ r_e \cdot sin(\varphi_b + inv\,\alpha_e) \end{pmatrix} \qquad 10$$

with the following elements:

- r_e :   radius with deviation

$$r_e = \sqrt{r_b^2 + l_{ye}^2} \qquad 11$$

- $inv\,\alpha_e$:   involute angle with deviation

$$inv\alpha_e = tan\left(\arccos\left(\frac{r_b}{r_e}\right)\right) - \arccos\left(\frac{r_b}{r_e}\right) \qquad 12$$

- l_{ye}:   length of roll with deviation

$$l_{ye} = l_y + \sum_{i=1}^{n}\left(a_i \cdot sin\left(2\pi \cdot l_y \cdot f_i - p_i\right)\right) \qquad 13$$

- a_i :   amplitude of wave i

- f_i :   frequency of wave i

- p_i :   phase of wave i

In Figure 12, a single waviness along the profile is shown. On the SAFT2w, three sinus waves were superimposed. The three chosen frequency values were in accordance with standard series of wavelengths (inverse of frequency) utilized in form measurement (Table 2) [37]. The amplitudes were chosen to get a peak-to-peak amplitude value < 20 µm.

Table 2 – Parameters of waviness definitions.

Harmonic, i	1	2	3
Frequency, f_i in mm^{-1}	0.125	0.4	1.25
Amplitude, a_i in µm	5	3	1
Phase, p_i in rad	0	0	0

6 Measurement of the artifact

6.1 Measurement procedure

Measurements of the external involute profile of the SAFT2w with the microprobe (Figure 13) in the MA and in the MC setup (3.3) were carried out on the GMI and compared. Through such measurements, the GMI provides the deviations between the measured profile and the nominal one (a mathematical perfect involute) over the length of roll. The obtained profile deviations were evaluated in two different ways over the length of roll ranging from 20 mm to 90 mm. First, a standard gear profile evaluation was carried out, where the profile slope deviation $f_{H\alpha}$, the profile form deviation $f_{f\alpha}$ and the total profile deviation F_{α} were computed. To characterize the waviness, a spectral analysis Fast Fourier Transformation (FFT) was performed and the three major peaks (frequency, f_i and amplitude, a_i) were determined. Each measurement was repeated three times. 2048 points were recorded over the total measurement length, which led to a sampling pitch of 50 µm over the length of roll.

The SAFT2w was placed and centered on the rotary table with the help of a probe indicator within a tolerance of ±2 µm. All measured profile deviations were determined with reference to the rotary table axis of the GMI and not to the *z*-axis of the artifact. Between the MA and the MC measurements, the artifact was removed from the machine and re-centered on the rotary table, which led to slightly different positions of the artifact. Moreover, the artifact's *z*-axis (defined in Figure 10) could not be determined, because the necessary measurements on the SAFT (the circle (2), the plane (3) and the hole (4), in Figure 10) could not be performed with the software used. As a consequence, the measurements could not be related to the artifact's *z*-axis. Therefore, additional measurements of the profile, named SMA and SMC measurements, were performed with the standard setup (use of only the P40 probing head with a conventional –Z stylus with a diameter of 3 mm, Figure 3b) after each measurement

with the microprobe without moving the artifact. That meant, it was possible to evaluate the resulting differences between the MA measurements and the MC measurements regardless of the position of the artifact by indirect comparisons of the SMA and the SMC measurements (both performed with the same standard setup).
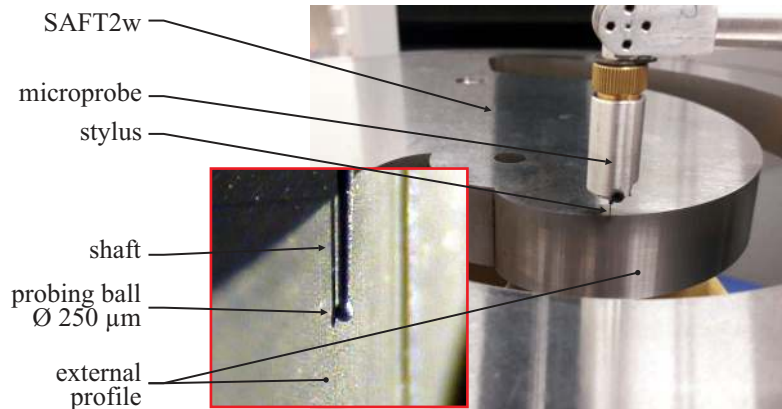

Figure 13 – Measuring the SAFT2w with the microprobe.

6.2   Gear evaluation

In Figure 14a, the measured profile of the external involute is presented for the MC measurement with the three deviation parameters $f_{H\alpha}$, $f_{f\alpha}$, and F_α of the gear evaluation. In Figure 14b, the profiles measured with both setups are displayed. MA and MC measurements slightly deviate at the beginning and at the end of the curves. For the SMA and the SMC measurements (Figure 14c), the same trend is observable. This can be directly related to the repositioning of the artifact mentioned before. To determine the three deviation parameters, a mean profile was determined by a best-fit method. The *profile slope deviation* $f_{H\alpha}$ corresponds to the distance between two copies of the nominal profile intersecting the extrapolated mean profile line at the profile control diameter and at the tip circle diameter. For the evaluation of the SAFT, both diameters have been set at the beginning and the end of the given evaluation range. The *profile form deviation $f_{f\alpha}$* is the distance between two parallel mean profiles including the measured profile over the evaluation range. The *total profile deviation F_α* is the distance

23

between two copies of the nominal profiles including the measured profile over the evaluation range. These definitions can be found in [38].

In Table 3, mean values (μ) and standard deviations (σ) of the gear parameters obtained from three measurements of the external involute profile are presented. The deviations between the MA and the MC mean values $\Delta\mu_M$ are also given. In a similar manner, the results of SMA and SMC measurements are also presented. The standard deviations obtained in MA and MC measurements do not exceed 0.1 µm, which proves a high repeatability. Furthermore, the standard deviations are almost identical to the ones obtained from SMA and SMC measurements. The observed differences between the MA and the MC measurements ($\Delta\mu_M$) are similar to the ones between the SMA and the SMC measurements ($\Delta\mu_S$) within a 0.2 µm tolerance. This indirectly proves that the MA and MC setups deliver identical results and initial deviations are only induced by the artifact repositioning, which was necessary for the switching between the two setups. The direct comparison between the MA and the SMA measurements, as well as between the MC and the SMC measurements reveals similar systematic differences ($E\mu$) within a tolerance of 0.1 µm. These negative differences show that the microprobe delivers "smaller" values than the standard setup, and that its characterization needs to be further investigated (4.1) in the future, leading to better measurements.
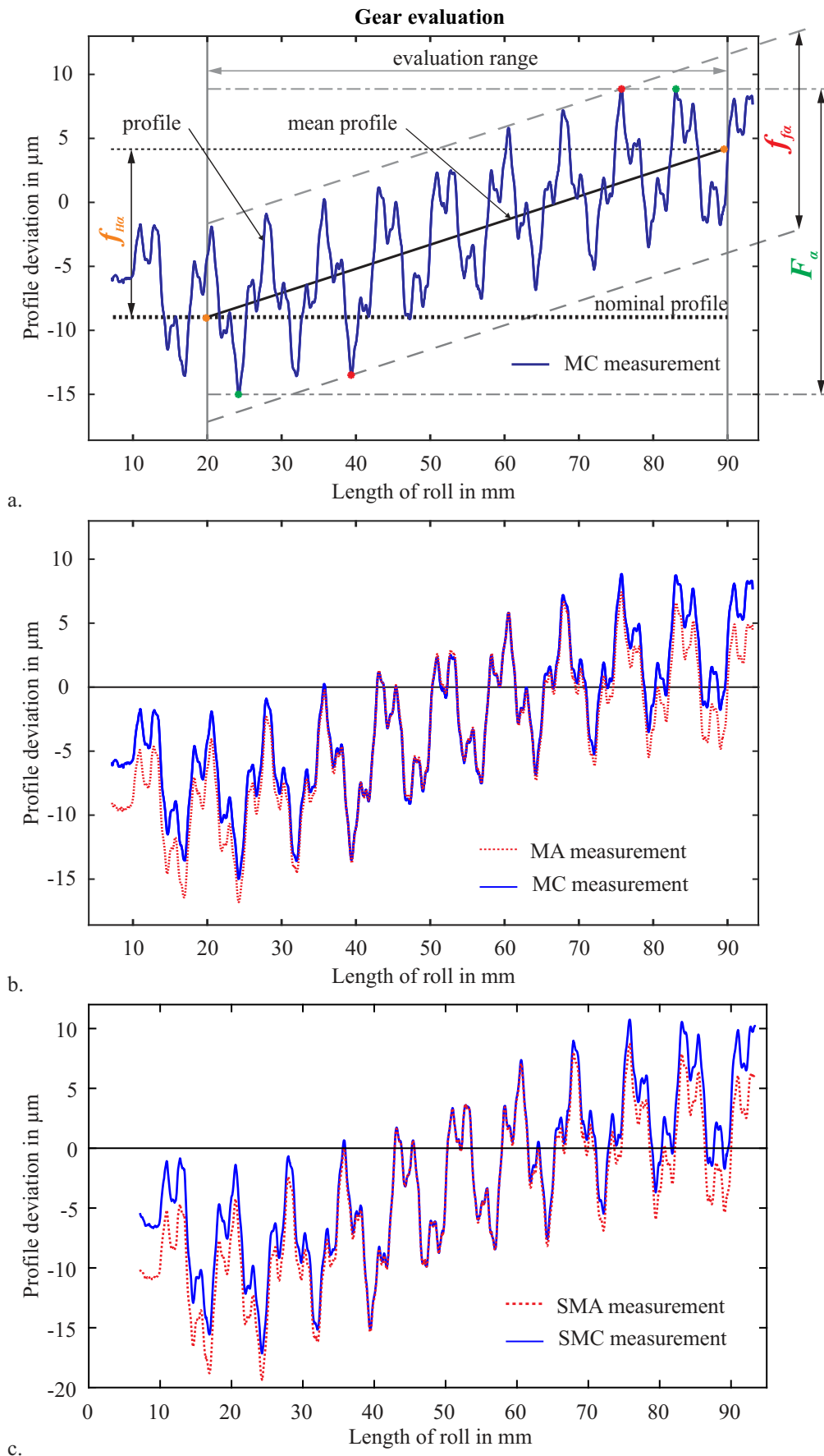
Figure 14 – a. MC measurement with the three deviation parameters typically used for gear evaluation $f_{H\alpha}$, $f_{f\alpha}$, and F_{α}, b. comparison of MA and MC measurements (obtained with the microprobe), and c. comparison of SMA and SMC measurements (obtained with the standard setup).

Table 3 – Gear evaluation results.

Measurement with the microprobe:

Gear parameters	MA measurement		MC measurement		Difference MA - MC
	μ_{MA}	σ_{MA}	μ_{MC}	σ_{MC}	$\Delta\mu_M = \mu_{MA} - \mu_{MC}$
$f_{H\alpha}$ in µm	12.1	0.1	13.3	0.1	-1.2
$f_{f\alpha}$ in µm	16.4	0.1	15.5	0.0	0.9
F_α in µm	24.2	0.1	23.9	0.1	0.3

Measurement with the standard setup:

Gear parameters	SMA measurement		SMC measurement		Difference SMA - SMC
	μ_{SMA}	σ_{SMA}	μ_{SMC}	σ_{SMC}	$\Delta\mu_S = \mu_{SMA} - \mu_{SMC}$
$f_{H\alpha}$ in µm	14.0	0.0	15.4	0.1	-1.4
$f_{f\alpha}$ in µm	19.1	0.1	18.1	0.3	1.0
F_α in µm	28.1	0.0	28.0	0.1	0.1

Systematic difference between measurements with microprobe and with standard setup

Gear parameters	$E\mu_A = \mu_{MA} - \mu_{SMA}$	$E\mu_C = \mu_{MC} - \mu_{SMC}$	$E\mu = \dfrac{(E\mu_A + E\mu_C)}{2}$
$f_{H\alpha}$ in µm	-1.9	-2.1	-2.0
$f_{f\alpha}$ in µm	-2.7	-2.6	-2.7
F_α in µm	-3.9	-4.1	-4.0

6.3 FFT evaluation

In Figure 15, FFTs of the MA and of the MC measurements of the external involute

profile are shown. Both results exhibit three peaks in the given evaluation range (0.05 to

1.3 mm^{-1}) including the nominal frequencies (Table 2).
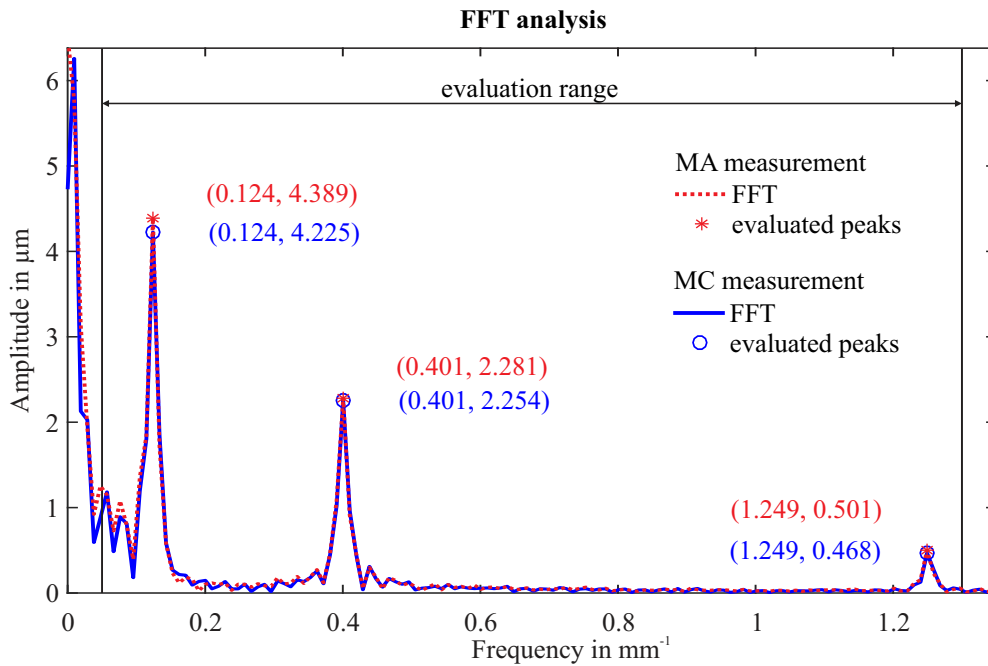
Figure 15 – FFT analysis of the measured profiles of the external involute with the numerical values of the frequency f_i, and the amplitude a_i for each observed peak for MA and MC measurement.

The FFT results for the MA, MC, SMA, and SMC measurements are summarized in Table 4. The listed mean values $\bar{f}_i$ of the frequencies and $\bar{a}_i$ of the amplitudes were obtained for each of the three measurements. The obtained peak positions are identical for all measurements and correspond well to the nominal values provided with the standard with less than 0.8 % deviation. The differences in peak amplitudes between the MA and the MC measurements (Δa_{iM}), and between the SMA and the SMC measurements (Δa_{iS}), are equal, which also proves the equivalence of the MA and the MC setups.

Similarly to the gear evaluation, a direct comparison between the MA and the SMA measurements, as well as between the MC and the SMC measurements reveals a systematic difference (Ea_i) which again shows that the microprobe seems to deliver "smaller" values than the standard setup.

Table 4 – FFT evaluation results

Measurement with the microprobe:

	MA measurement		MC measurement		Difference MA - MC
i	f_i in Hz	a_i in µm	f_i in Hz	a_i in µm	
	$\bar{f}_{iMA}$	$\bar{a}_{iMA}$	$\bar{f}_{iMC}$	$\bar{a}_{iMC}$	$\Delta a_{iM} = \bar{a}_{iMA} - \bar{a}_{iMC}$
1	0.124	4.4	0.124	4.2	0.2
2	0.401	2.3	0.401	2.3	0.0
3	1.249	0.5	1.249	0.5	0.0

Measurement with the standard setup:

	SMA measurement		SMC measurement		Difference SMA - SMC
i	f_i in Hz	a_i in µm	f_i in Hz	a_i in µm	
	$\bar{f}_{iSMA}$	$\bar{a}_{iSMA}$	$\bar{f}_{iSMC}$	$\bar{a}_{iSMC}$	$\Delta a_{iS} = \bar{a}_{iSMA} - \bar{a}_{iSMC}$
1	0.124	5.1	0.124	4.9	0.2
2	0.401	2.6	0.401	2.6	0.0
3	1.249	0.6	1.249	0.6	0.0

Systematic difference between measurements with microprobe and with standard setup

i	$Ea_{iA} = \bar{a}_{iMA} - \bar{a}_{iSMA}$	$Ea_{iC} = \bar{a}_{iMC} - \bar{a}_{iSMC}$	$Ea_{iC} = \dfrac{(Ea_{iA} + Ea_{iC})}{2}$
1	-0.7	-0.7	-0.7
2	-0.4	-0.4	-0.4
3	-0.1	-0.1	-0.1

7 Conclusion and outlook

In this work, the assembly, the characterization and the successful integration of a

silicon-based microprobe in the coordinate measuring machine GMI is reported in

detail.

The SMD soldering or assembly of the microprobe on a PCB offers a very good fixing

and contacting solution. The new adapter with its plugging and screwing system makes

it easy and safe to change the microprobe. More measurement tasks are permitted with

the two possible different orientations of the microprobe.

The combination of the microprobe and the probing system of the GMI (MC setup)

presents more advantages than solely using the microprobe (MA setup). The use, the

installation of the microprobe and the exchange between the microprobe and the

standard stylus are made easier. Thanks to a flexible connection, this new mounting

28

setup was tested, where the two probing systems, the microprobe and the probing head of the GMI, are used simultaneously. Through this combination, the anisotropic property and the limited deflection ranges of the microprobe can be partly compensated. Moreover, there is no need to re-run the referencing after each change between the microprobe and the standard stylus, which permits an automatic change. The evaluation of the combined setup and the microprobe used alone shows that both present the same properties. A verification measurement carried out on an involute waviness scanning artifact also reveals comparable results between the two setups. This equivalence, the advantage of a process allowing easy exchanges and the compensation of some limiting properties of the microprobe (anisotropy, limited deflections range), speak in favor of the combination of the two probing systems. Moreover, the simple characterization process and the standard referencing procedure of the microprobe on the machine enable its fast preparation.

Future work will concentrate on the optimization of the characterization in order to permit correct 3D measurements. Furthermore, microprobe designs with reduced or even unneglectable anisotropy are currently being investigated to avoid problems with the sliding of the probing ball and resulting uncertainties.

8 Acknowledgment

9 References

[1] Weckenmann A, Estler T, Peggs G, McMurtry D. Probing systems in dimensional metrology. CIRP Annals - Manufacturing Technology 2004;53(2):657–84. doi: 10.1016/S0007-8506(07)60034-1.

[2] Weckenmann A, Peggs GN, Hoffmann J. Probing systems for dimensional micro- and nano-metrology. Meas. Sci. Technol. 2006;17(3):504–9. doi: 10.1088/0957-0233/17/3/S08.

[3] Masuzawa T, Hamasaki Y, Fujino M. Vibroscanning Method for Nondestructive Measurement of Small Holes. CIRP Annals - Manufacturing Technology 1993;42(1):589–92. doi: 10.1016/S0007-8506(07)62516-5.

[4] Masuzawa T, Kim BJ, Bergaud C, Fujino M. Twin-Probe Vibroscanning Method for Dimensional Measurement of Microholes. CIRP Annals 1997;46(1):437–40. doi: 10.1016/S0007-8506(07)60860-9.

[5] Goj B, Dressler L, Hoffmann M. Design and characterization of a resonant triaxial microprobe. J. Micromech. Microeng. 2015;25(12):125011. doi: 10.1088/0960-1317/25/12/125011.

[6] MITUTOYO, UMAP Vision System; Available from: http://www.mitutoyo.co.jp/eng/.

[7] Claverley JD, Leach RK. Development of a three-dimensional vibrating tactile probe for miniature CMMs. Precision Engineering 2013;37(2):491–9. doi: 10.1016/j.precisioneng.2012.12.008.

[8] Neuschaefer-Rube U, Bremer H, Hopp B, Christoph R. Recent developments of the 3D fiber probe. 11th Laser Metrology for Precision Measurement and Inspection in Industry. Tsukuba, Japan; 2014.

[9] Schwenke H, Wäldele F, Weiskirch C, Kunzmann H. Opto-tactile sensor for 2D and 3D measurement of small structures on coordinate measuring Machines. CIRP

Annals - Manufacturing Technology 2001;50(1):361–4. doi: 10.1016/S0007-8506(07)62140-4.

[10] Linz S, Schoch A, Bach C, Ettemeyer A, Hopp B, Andras M. 3D fiber probe: State of the art and new developments. In: Bellouard Y, editor. International Symposium on Optomechatronic Technologies (ISOT), 2012: 29 - 31 Oct. 2012, Paris, France. Piscataway, NJ: IEEE; 2012, p. 1–4. ISBN: 978-1-4673-2877-7. doi: 10.1109/ISOT.2012.6403236.

[11] Muralikrishnan B, Stone JA, Stoup JR. Fiber deflection probe for small hole metrology. Precision Engineering 2006;30(2):154–64. doi: 10.1016/j.precisioneng.2005.07.004.

[12] Peggs GN, Lewis AJ, Oldfield S. Design for a compact high-accuracy CMM. CIRP Annals - Manufacturing Technology 1999;48(1):417–20. doi: 10.1016/S0007-8506(07)63216-8.

[13] Lewis AJ. Fully traceable miniature CMM with submicrometer uncertainty. In: Optics & Photonics, Proc. SPIE 5190, Recent Developments in Traceable Dimensional Measurements II. SPIE; 2003, p. 265–276. doi: 10.1117/12.503349.

[14] Leach RK, Haycocks J, Jackson K, Lewis AJ, Oldfield S, Yacoot A. Advances in traceable nanometrology at the National Physical Laboratory. INSTITUTE OF PHYSICS PUBLISHING 2001. doi: 10.1088/0957-4484/12/1/201.

[15] Peggs GN, Lewis AJ, Leach RK. Measuring the metrology gap – three dimensional metrology at the mesoscopic level. Journal of Manufacturing Processes 2004;6(1):117–24. doi: 10.1016/S1526-6125(04)70065-1.

[16] Bos EJC. Tactile 3D probing system for measuring MEMS with nanometer uncertainty:aspects of probing, design, manufacturing and assembly. Technische Universiteit Eindhoven; 2008. ISBN: 978-90-386-1216-4.

[17] Bos EJC, Heldens RWP, Delbressine FLM, Schellekens PHJ, Dietzel A. Compensation of the anisotropic behavior of single crystalline silicon in a 3D tactile sensor. Sensors and Actuators A: Physical 2007;134(2):374–81. doi: 10.1016/j.sna.2006.05.043.

[18] Bos EJC. Aspects of tactile probing on the micro scale. Precision Engineering 2011;35(2):228–40. doi: 10.1016/j.precisioneng.2010.09.010.

[19] Bütefisch S, Büttgenbach S, Kleine-Besten T, Brand U. Micromechanical three-axial tactile force sensor for micromaterial characterisation. Microsystem Technologies 2001;7(4):171–4. doi: 10.1007/s005420000083.

[20] Bütefisch S, Solzbacher F, Ziermann R, Krause P, Büttgenbach S, Wilke R et al. Mikrotaster für Anwendungen in der taktilen Wegmesstechnik (Micro Probe for Dimensional Metrology). Technisches Messen 2003(70). doi: 10.1524/teme.70.5.238.20049.

[21] Phataralaoha A. Entwicklung piezoresistiver taktiler Sensoren für die Charakterisierung von Mikrokomponenten. Aachen: Shaker; 2009. ISBN: 3832284443.

[22] Tibrewala A, Phataralaoha A, Büttgenbach S. Analysis of full and cross-shaped boss membranes with piezoresistors in transversal strain configuration. J. Micromech. Microeng. 2008;18(5):55001. doi: 10.1088/0960-1317/18/5/055001.

[23] Ferreira N, Brennecke A, Dietzel A, Buttgenbach S, Krah T, Metz D et al. Reducing the probe ball diameters of 3D silicon-based microprobes for dimensional metrology. In: 2013 Seventh International Conference on Sensing Technology (ICST). IEEE; 2013, p. 301–306. ISBN: 978-1-4673-5222-2. doi: 10.1109/ICSensT.2013.6727663.

[24] Ferreira N, Krah T, Jeong DC, Metz D, Kniel K, Dietzel A et al. Integration of a silicon-based microprobe into a gear measuring instrument for accurate

measurement of micro gears. Meas. Sci. Technol. 2014;25(6):64016. doi: 10.1088/0957-0233/25/6/064016.

[25] Zeiss. Datasheet F25; Available from: centerfreeformoptics.org/wp-content/uploads/2014/08/f25_brochure.pdf.

[26] Ferreira N. Entwicklung, Integration und Erprobung eines piezoresistiven 3D-Mikrotasters. Dissertation. Aachen: Shaker; 2015. ISBN: 9783844035469.

[27] Ferreira N, Krah T, Kniel K, Büttgenbach S, Härtig F. Universal characterization method for 3D tactile probing systems. In: International Symposium on Precision Engineering Measurement and Instrumentation 2012. SPIE; 2013, p. 875–945. doi: 10.1117/12.2011702.

[28] Klingelnberg GmbH. P40 - KLINGELNBERG Precision Measuring Center; Available from: https://www.klingelnberg.com/.

[29] Richter C, Krah T, Büttgenbach S. Novel 3D manufacturing method combining microelectrial discharge machining and electrochemical polishing. Microsyst Technol 2012;18(7-8):1109–18. doi: 10.1007/s00542-012-1452-x.

[30] Ferreira N, Metz D, Dietzel A, Buttgenbach S, Krah T, Kniel K et al. 3D micro probing systems for gear measurements with nanometer-scale deviation. In: 2013 International Conference on Manipulation, Manufacturing and Measurement on the Nanoscale (3M-NANO): 26 - 30 Aug. 2013, Suzhou, China. Piscataway, NJ: IEEE; 2013, p. 253–258. ISBN: 978-1-4799-1213-1. doi: 10.1109/3M-NANO.2013.6737426.

[31] Metz D, Dietzel A. New parallelogram 3D-displacement sensor for micro probing and dimensional metrology. In: Transducers'17, Kaohsiung: The 19th International Conference on Solid-State Sensors, Actuators and Microsystems June 18-22, 2017, Kaohsiung, Taiwan. Piscataway, NJ: IEEE; 2017, p. 982–985. ISBN: 978-1-5386-2732-7. doi: 10.1109/TRANSDUCERS.2017.7994215.

[32] VDI/VDE 2612. Profile and helix checking of involute cylindrical gears.

[33] VDI/VDE 2613. Pitch and runout testing on gearings cylindrical gears, whormwheels, bevel gears.

[34] Metz D, Ferreira N, Dietzel A. 3D piezoresistive silicon microprobes with stacked suspensions for tailored mechanical anisotropies. Sensors and Actuators A: Physical 2017;267:164–76. doi: 10.1016/j.sna.2017.09.039.

[35] Härtig F, Krystek M, Klein S. Reliable detection of periodic micro structures on open surfaces. Key Engineering Materials 2008(381-382):15–8. doi: 10.4028/www.scientific.net/KEM.381-382.15.

[36] DIN ISO 21771. Gears – Cylindrical involute gears and gear pairs – Concepts and geometry; 2007.

[37] DIN EN ISO 12780-2. Geometrical product specifications (GPS) – Straightness – Part 2: Specification operators; 2011.

[38] DIN ISO 1328-1. Cylindrical gears – ISO system of flank tolerance classification – Part 1: Definitions and allowable values of deviations relevant to flanks of gear teeth; 2013.

10 List of tables

11 List of figures